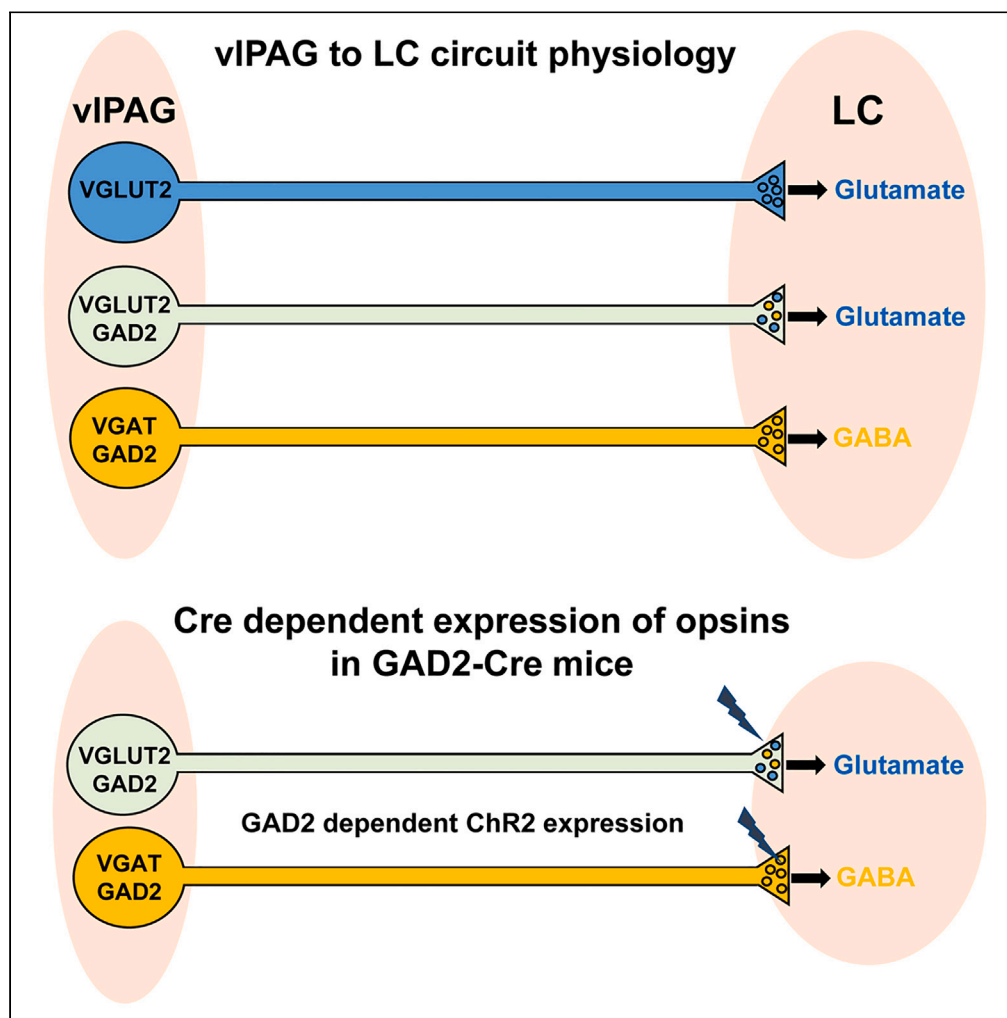


## Article

## Expression of GAD2 in excitatory neurons projecting from the ventrolateral periaqueductal gray to the locus coeruleus



Erika K. Harding,  
Zizhen Zhang, Julia  
Canet-Pons, Sierra  
Stokes-Heck, Tuan  
Trang, Gerald W.  
Zamponi

zamponi@ucalgary.ca

#### Highlights

A subpopulation of vIPAG-LC projecting neurons expresses both glutamate and GABA

These neurons express GAD2, but not VGAT and cannot support vesicular GABA release

The GAD2 promoter cannot be used to selectively express opsins in vIPAG GABA cells

Harding et al., iScience 27,  
109972  
June 21, 2024 © 2024 The  
Author(s). Published by Elsevier  
Inc.  
[https://doi.org/10.1016/  
j.isci.2024.109972](https://doi.org/10.1016/j.isci.2024.109972)

## Article

## Expression of GAD2 in excitatory neurons projecting from the ventrolateral periaqueductal gray to the locus coeruleus

Erika K. Harding,<sup>1,2,3,4</sup> Zizhen Zhang,<sup>1,3,4</sup> Julia Canet-Pons,<sup>2,3</sup> Sierra Stokes-Heck,<sup>2,3</sup> Tuan Trang,<sup>2,3</sup> and Gerald W. Zamponi<sup>1,3,5,\*</sup>

## SUMMARY

**The ventrolateral periaqueductal gray (vlPAG) functionally projects to diverse brain regions, including the locus coeruleus (LC). Excitatory projections from the vlPAG to the LC are well described, while few studies have indicated the possibility of inhibitory projections. Here, we quantified the relative proportion of excitatory and inhibitory vlPAG-LC projections in male and female mice, and found an unexpected overlapping population of neurons expressing both GAD2 and VGLUT2. Combined *in vitro* optogenetic stimulation and electrophysiology of LC neurons revealed that vlPAG neurons expressing channelrhodopsin-2 under the GAD2 promoter release both GABA and glutamate. Subsequent experiments identified a population of GAD2+/VGLUT2+ vlPAG neurons exclusively releasing glutamate onto LC neurons. Altogether, we demonstrate that ~25% of vlPAG-LC projections are inhibitory, and that there is a significant GAD2 expressing population of glutamatergic projections. Our findings have broad implications for the utility of GAD2-Cre lines within midbrain and brainstem regions, and especially within the PAG.**

## INTRODUCTION

The ventrolateral periaqueductal gray (vlPAG) receives descending information from the cortex and other brain structures to drive responses to salient stimuli. These include coordination of the fight, flight, or freeze response, regulating wakefulness and arousal, and modulating pain through descending projections to the rostral ventromedial medulla (RVM) and locus coeruleus (LC).<sup>1–6</sup> Projections from the vlPAG to LC have been functionally and anatomically characterized, but the nature and relative strength of this projection is not well defined.<sup>2,7–9</sup> Notably, these projections have traditionally been thought to be predominantly excitatory, but a significant number of projections have been identified as putative inhibitory projections due to expression of the inhibitory marker Glutamate decarboxylase 2 (GAD2).<sup>10</sup>

Glutamate decarboxylase 1 (GAD1, GAD67) and Glutamate decarboxylase 2 (GAD2, GAD65) are enzymes critical for synthesis of GABA from glutamate.<sup>11</sup> While both enzymes synthesize GABA, GAD1 is generally located in the cytoplasm, and GAD2 is localized more toward axon terminals. GAD1 and GAD2 are generally coexpressed in GABAergic neurons, as confirmed by immunohistochemical and *in situ* hybridization.<sup>12</sup> Whereas GAD1 and GAD2 are essential for synthesis of GABA, the vesicular GABA transporter (VGAT) is essential for packaging GABA into vesicles for synaptic release.<sup>13</sup> Because of the ubiquitous presence of GAD2 in GABAergic neurons, and role in synthesizing GABA at axon terminals for synaptic release, GAD2-Cre mice were developed to drive Cre recombinase expression selectively in GABAergic neurons.<sup>14</sup> Expression of Cre recombinase was determined to be restricted to GABAergic neurons through colocalization with GAD67 and/or GABA and displayed high colocalization in a number of brain regions.<sup>14,15</sup>

However, recent studies have demonstrated the capacity for neurons in brain regions such as the ventral tegmental area, entopeduncular nucleus, and dentate gyrus during development to corelease GABA and glutamate.<sup>16–19</sup> Moreover, the expression of GAD2 has been identified previously in vesicular glutamate transporter 2 (VGLUT2) containing neurons of the lateral habenula, while the lack of VGAT suggests these neurons may only synaptically release glutamate.<sup>20</sup> Indeed, electrophysiological characterization of the output of these neurons indicates the selective synaptic release of glutamate, but not GABA. Furthermore, scRNA-seq of the preoptic area of the hypothalamus has also revealed the overlap of mRNA for VGLUT2 and GAD2, but not VGAT, in these neurons,<sup>21</sup> and crossing of GAD65 and VGAT transgenic lines has demonstrated a significant number of GAD65+/VGAT-neurons in the lateral hypothalamus.<sup>22</sup> Thus, in some brain regions, expression of GAD2 may not be sufficient to isolate GABAergic populations of neurons.

<sup>1</sup>Department of Clinical Neurosciences, University of Calgary, Calgary, AB T2N 4N1, Canada

<sup>2</sup>Faculty of Veterinary Medicine, University of Calgary, Calgary, AB T2N 4N1, Canada

<sup>3</sup>Hotchkiss Brain Institute, University of Calgary, Calgary, AB T2N 4N1, Canada

<sup>4</sup>These authors contributed equally

<sup>5</sup>Lead contact

\*Correspondence: zamponi@ucalgary.ca

<https://doi.org/10.1016/j.isci.2024.109972>



When driving channelrhodopsin-2 (ChR2) expression in vPAG neurons using GAD2-Cre mice to characterize potential functional vPAG inhibitory input to the LC, we found that optically evoked postsynaptic currents in LC neurons contained both inhibitory and excitatory monosynaptic components. Using *in vitro* optogenetics, electrophysiology, immunohistochemistry, and *in situ* hybridization, we demonstrate that in LC projecting vPAG neurons, a subpopulation of neurons coexpresses GAD2 and VGLUT2, but produces only excitatory postsynaptic release due to a lack of VGAT expression. Using VGLUT2-cre and VGAT-cre lines to drive expression of ChR2 in vPAG neurons showed excitatory and inhibitory postsynaptic current selectivity, respectively. This study defines the potential caveats of GAD2-Cre transgenic lines, confirms the exclusivity of VGLUT2-cre and VGAT-cre transgenic lines within the vPAG, and highlights the necessity to confirm exclusivity of expression in each brain region and projection studied.

## RESULTS

### Optogenetic stimulation of GAD2+ afferents from the vPAG yields both inhibitory and excitatory postsynaptic responses in LC neurons

To determine if inhibitory neurons from the vPAG mediate functional inhibition of LC neurons, a viral vector was injected into the right vPAG to drive expression of channelrhodopsin-2 (ChR2) in a Cre-dependent manner (AAV-DIO-ChR2-YFP). 8–10 weeks after injection, brain slices containing the LC were obtained from these mice and recordings were made from the ipsilateral LC, where the majority of YFP fluorescence was present. Within the recording pipette we included Alexa Fluor 555 to allow for post-recording identification of recorded neurons and confirmation that TH + LC neurons were recorded (Figures 1A and 1B). Brief pulses of 473 nm laser light (5 ms) from an optical fiber placed near the recording site were used to evoke postsynaptic currents in the recorded neuron. Holding at 0 mV yielded optically evoked inhibitory postsynaptic currents (oIPSCs) in 61.5% of LC neurons ( $n = 52$  total recorded neurons). However, when the holding potential was lowered to  $-60$  mV, in 80.8% of neurons an apparent optically evoked excitatory postsynaptic current (oEPSC) was also noted. Recorded neurons could be divided into three groups; those with only an oIPSC, those with both an oIPSC and oEPSC, and those with only an oEPSC (Figures 1C and 1D).

Latencies of oIPSCs and oEPSCs averaged less than 3 ms regardless of the nature of the optically evoked current, suggesting that all recorded events were likely monosynaptic (Figure 1E), and average amplitude was typically less than 200 pA (Figure 1F). To assess whether both oIPSCs and oEPSCs are monosynaptic in nature, tetrodotoxin (TTX) was first washed onto a neuron to eliminate vesicular release, and then monosynaptic release of both oIPSCs and oEPSCs was rescued with perfusion of 4-AP in the presence of TTX (Figure 1G). Together, this indicates that currents recorded at  $-60$  mV and 0 mV are both monosynaptic. Next, we performed systematic perfusion of Bicuculline to block GABA<sub>A</sub> receptors and DNQX to block AMPA receptors. When Bicuculline was perfused onto the slice first, the oIPSC at 0 mV was eliminated, with the oEPSC at  $-60$  mV remaining intact. Subsequent addition of DNQX then eliminated the oEPSC (Figure 1H). In the converse experiment in which DNQX was perfused first, the oEPSC was eliminated, followed by blocking of the oIPSC when Bicuculline was additionally perfused (Figure 1I). We therefore conclude that ChR2 activation of GAD2+ vPAG afferents onto LC neurons produce release of both GABA, as expected, but also glutamate, with monosynaptic properties and no dependence on the presence of the opposing neurotransmitter release.

### CTB-488 tracing of the vPAG to LC pathway reveals vPAG neurons that colocalize with markers of inhibitory and excitatory neurons

To further characterize the projections from the vPAG to LC, we injected the retrograde tracer Cholera Toxin Subunit B-488 (CTB-488) into the LC of GAD2-Cre mice that had been crossed with the ai9 reporter line, such that GAD2+ neurons were tdTomato+ (Figure 2A). Mice were perfused three weeks after CTB-488 injection, and immunohistochemistry with a CaMKII antibody was performed to label the cell bodies of excitatory neurons in the vPAG. CaMKII was chosen based on localization to the cell body, therefore avoiding filling the dense neuropil of the vPAG with fluorescence. CTB-488 injection of the LC produced predominant ipsilateral fluorescence throughout the vPAG, in areas spanning from bregma  $-5.0$  to  $-4.2$  (Figure 2B). 4-colour colocalization of DAPI, CTB-488, tdTomato, and CaMKII revealed three populations of LC-projecting vPAG neurons: those expressing only GAD2, those expressing only CaMKII, and those expressing both GAD2 and CaMKII (Figures 2C and 2D). Importantly, no such overlap was observed in the dentate gyrus, where tdTomato fluorescence was separate and restricted from CaMKII+ neurons (Figures 2E–2G).

Overall, we found that most projections to the LC originate from more central areas of the vPAG (bregma  $-4.5$  to  $4.7$ ) (Figure 2H), and that the vast majority of projections were solely CaMKII+, and therefore likely to be excitatory. Conversely, the GAD2+ population of projections comprised 25.8% of all projections, with the intersectional population of GAD2+/CaMKII+ projection neurons comprising 21.4% of all projections to the LC (Figure 2I). Since CaMKII has been noted to be present in some inhibitory neurons,<sup>23–25</sup> CaMKII was validated by examining colocalization in VGLUT2-cre x ai9 mice in the vPAG, with 93.3% of CaMKII+ neurons being tdTomato+, unlike colocalization with a glutaminase antibody, where only 60.4% of glutaminase+ neurons were tdTomato+ (Figure S1). Additionally, immunohistochemistry against GABA was also performed in VGLUT2-cre x ai9 mice which were injected with CTB-488 into the LC (Figure S2). Here, we found an intersectional population of 12.7% of LC projecting neurons in the vPAG that were both VGLUT2+ and GABA+. Together, the colocalization of both CaMKII and GAD2, and VGLUT2 and GABA in  $\sim 10$ – $20\%$  of all vPAG to LC projections indicates the presence of a population of neurons that expresses VGLUT2, but also expresses GAD2 and produces GABA.

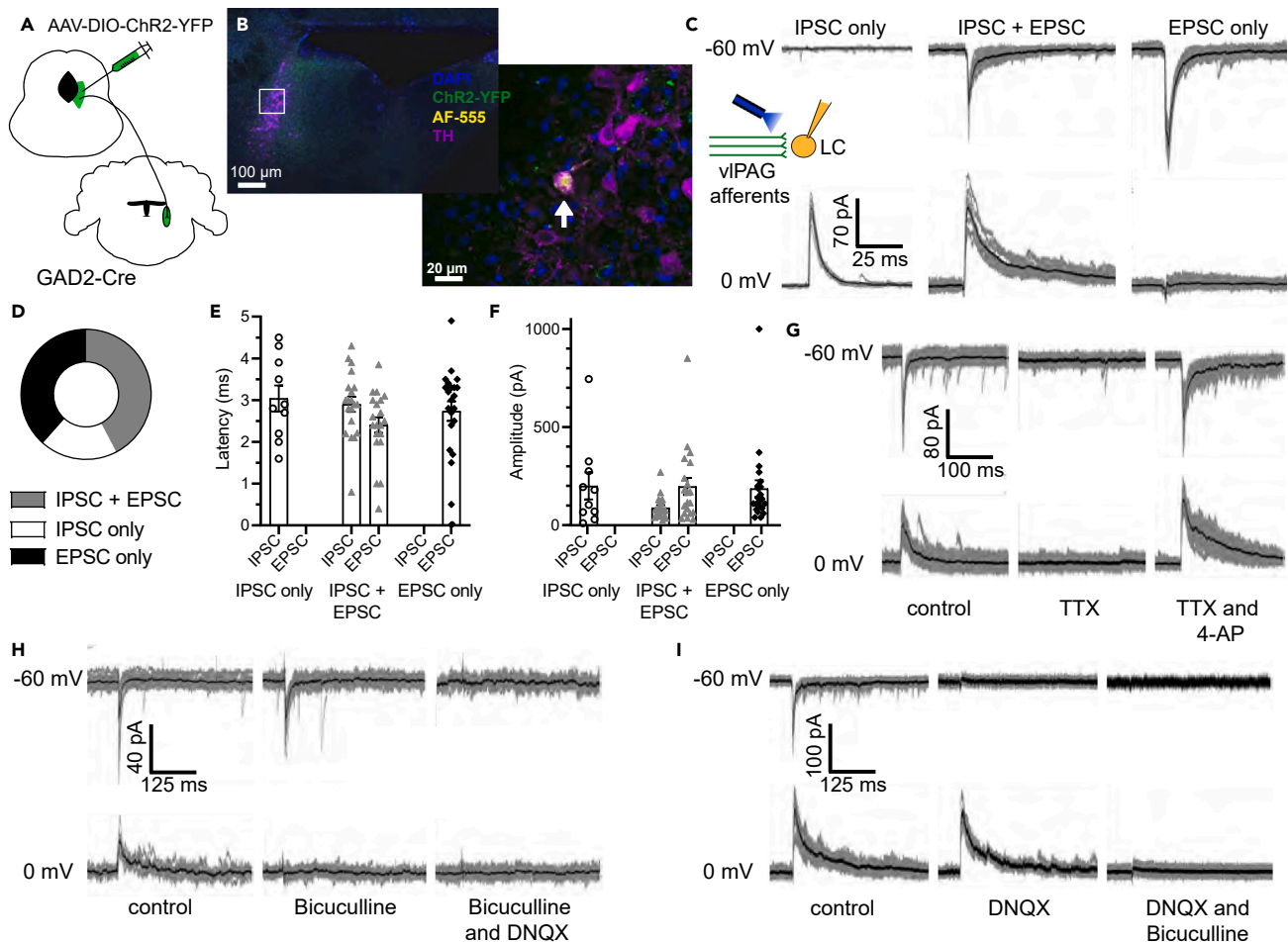


**Figure 1. Optogenetic stimulation of GAD2+ afferents from the vPAG yields both inhibitory and excitatory postsynaptic responses in LC neurons**

(A) Schematic of electrophysiological recording paradigm.  
 (B) Post-hoc immunohistochemistry confirming TH + identity of a recorded locus coeruleus (LC) neuron.  
 (C and D) Optical stimulation of vPAG afferents yielded three types of postsynaptic response; IPSC only, IPSC and EPSC, or EPSC only. (C) Representative traces of each type of postsynaptic response (black = average trace, gray = individual sweeps). (D) Proportion of types of responses in 52 recorded LC neurons (IPSC only = 10 neurons from 6 mice, IPSC and EPSC = 20 neurons from 10 mice, EPSC only = 22 neurons from 10 mice).  
 (E) Average latency of optically evoked response in each neuron.  
 (F) Average amplitude of optically evoked response in each neuron.  
 (G) Representative trace of a neuron which contained optically evoked IPSCs and EPSCs, demonstrating block of response by TTX and rescue by TTX + 4-AP perfusion.  
 (H) Representative trace demonstrating successive block of IPSC and EPSC by Bicuculline and DNQX, respectively.  
 (I) Representative trace demonstrating successive block of EPSC and IPSC by DNQX and Bicuculline, respectively. All error bars reflect S.E.M.

### Colocalization of GABA and CaMKII is present in vPAG to LC projecting neurons in both male and female mice

Given that all experiments above were performed in male mice, and sex differences in vPAG circuitry and function have been previously reported,<sup>26–28</sup> we next determined if the number of projecting neurons to the LC, the rostrocaudal distribution, or the presence of this inter-sectional population of neurons containing markers for both excitatory and inhibitory neurons differed based on sex. Female and male C57Bl/6 mice were each injected with CTB-488 into the right LC. Due to the difference in size of female mice, coordinates of the LC injection site were shifted to better align with the location of the female LC, and confirmed with post-hoc imaging of the LC (Figures 3A and 3B).

Comparison of the average number of CTB+ neurons per vPAG slice, and the rostrocaudal distribution of these neurons revealed no significant differences between sexes ( $p = 0.150$ ) (Figure 3C). In an observational analysis of a subset of these mice, immunostaining against CaMKII and GABA revealed the existence of the inter-sectional population of neurons expressing both CaMKII and GABA in 24.2% of vPAG to LC projecting neurons in male mice, and in 21.7% of neurons in female mice (Figure 3D). In slices from both males and females, whereas robust colocalization of CaMKII and GABA was observed in the vPAG, no such colocalization was observed in the dentate gyrus (Figures 3E and 3F).

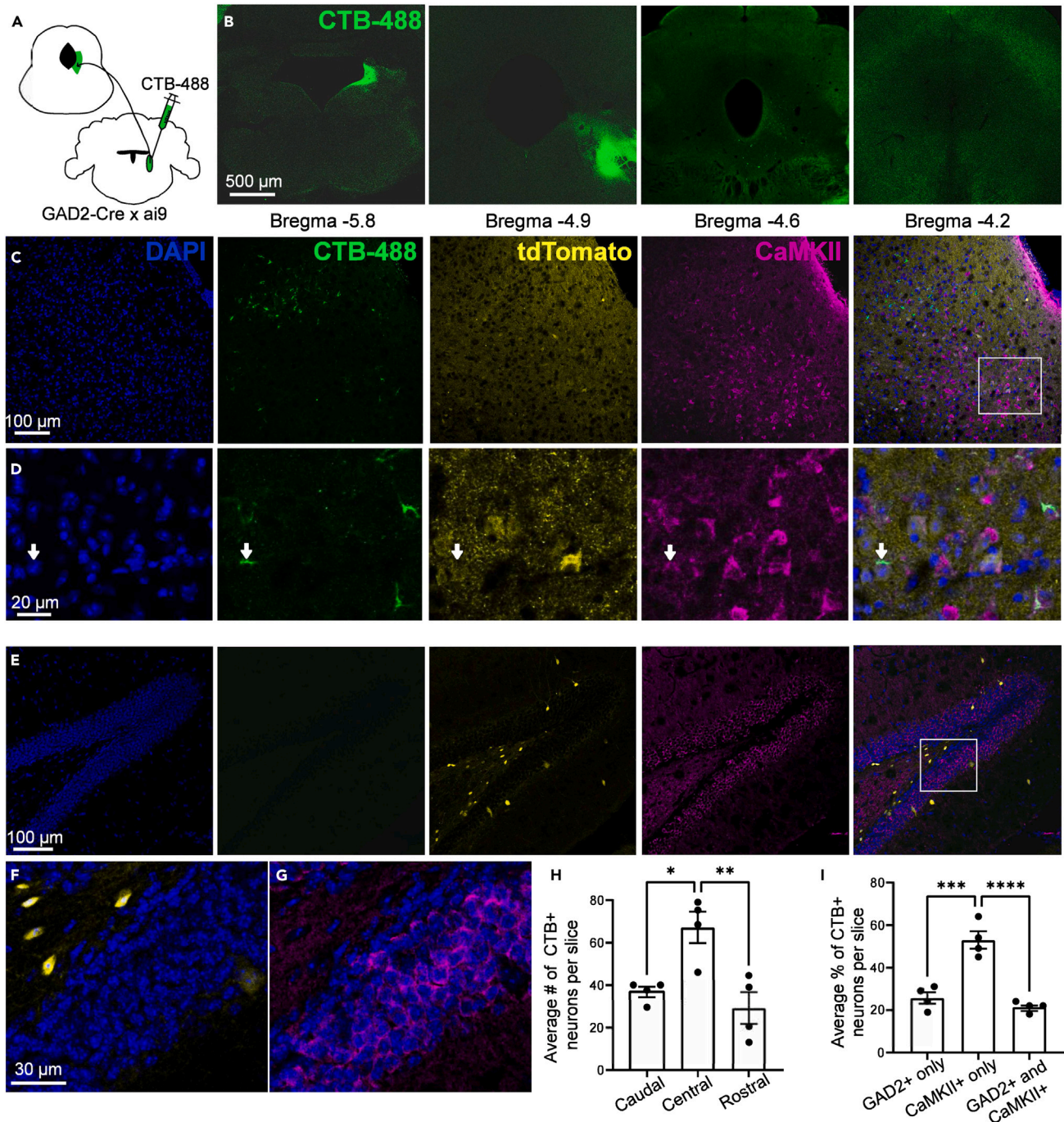


**Figure 2. CTB-488 Tracing of the vPAG to LC pathway reveals vPAG neurons that coexpress GAD2 and CaMKII**

(A) Schematic of CTB-488 tracing paradigm.  
 (B) Low magnification images demonstrating injection location in the LC (left panel) and distribution of CTB+ neurons (green) throughout the ventrolateral periaqueductal gray (vPAG) (right 3 panels).  
 (C) Representative image of immunohistochemical staining of vPAG neurons. GAD2 expression defined by tdTomato expression as driven by crossing of the GAD2-Cre and ai9 mouse lines.  
 (D) Magnified image of C as delineated by white rectangle. Arrows indicate CTB+ neurons expressing both GAD2 and CaMKII.  
 (E) Comparative image of immunohistochemical staining in the dentate gyrus.  
 (F and G) Magnified images of (E) as delineated by white rectangle, showing separate GAD2 and CaMKII expression in the dentate gyrus.

**Figure 2. Continued**

(H) Average distribution of CTB+ neurons in the rostrocaudal axis in the vPAG (N = 1009 neurons from 22 slices/4 mice) (Caudal = bregma  $-4.8$  to  $-5.0$ , Central =  $-4.5$  to  $-4.7$ , Rostral =  $-4.2$  to  $-4.4$ ). One-way ANOVA  $p = 0.0046$ , Sidak's post-hoc comparisons.

(I) Average % of CTB+ neurons expressing GAD2 only, both GAD2 and CaMKII, or CaMKII only (N = 810 neurons from 22 slices/4 mice). One-way ANOVA  $p < 0.0001$ , Sidak's post-hoc comparisons. Individual points represent averages from each mouse. \* $p < 0.05$ , \*\* $p < 0.01$ , \*\*\* $p < 0.001$ , \*\*\*\* $p < 0.0001$ . All error bars denote S.E.M.

**In situ hybridization of vPAG to LC projecting neurons reveals a subpopulation of neurons that express both GAD2 and VGLUT2, but not VGAT**

We next determined the nature of vPAG neurons that express both excitatory and inhibitory markers. We initially hypothesized that these cells might support co-release of GABA and glutamate since neurons capable of such dual release had previously been identified in other brain areas.<sup>19</sup> However, the existence of LC neurons that received only oEPSCs from GAD2+ vPAG afferents indicates this may not be the case. Instead, it is possible that this population expresses GAD2 and produces GABA, but is not capable of GABA vesicular release, as previously noted in a subpopulation of excitatory neurons in the lateral habenula.<sup>20</sup> Thus, we performed *in situ* hybridization of vPAG slices from C57Bl/6 mice injected with CTB-488 into the right LC. We probed for three types of mRNA: VGLUT2, GAD2, and VGAT.

As expected, many vPAG to LC projections were VGLUT2+, or GAD2+ and VGAT+, representing classical excitatory and inhibitory neurons, respectively. A number of neurons were also VGLUT2+ and GAD2+, but VGAT- (Figures 4A–4D; Figure S3). We found these non-classical excitatory neurons in both LC projecting and non-LC projecting vPAG neurons (Figures 4C and 4D). When quantifying the LC-projecting vPAG neurons, this population comprised 21.5% of all projections, in close agreement with our immunohistochemistry results (Figure 4E).

Importantly, as with our immunohistochemistry data, no overlap of VGLUT2 and GAD2 was observed in dentate gyrus neurons, nor were any neurons positive for GAD2, but lacking VGAT (Figures 4F and S3A). As a final control, RNAscope was performed in GAD2-Cre mice, probing for GAD2 and Cre mRNA. In this experiment, we found that essentially no neurons expressed Cre in the absence of GAD2, ruling out the possibility of ectopic Cre expression in the GAD2-Cre transgenic line (Figure S4). These results are thus consistent with our electrophysiological characterization of GAD2+ vPAG afferents, indicating the presence of GAD2 in some VGLUT2+ vPAG neurons, such that activating afferents from the vPAG could conceivably activate only inhibitory GAD2+ afferents, only excitatory GAD2+/VGLUT2+ afferents, or a combination of both.

**Optogenetic stimulation of VGLUT2+ and VGAT+ afferents from the vPAG yields exclusively excitatory or inhibitory postsynaptic responses in LC neurons**

As a final confirmation of the selectivity of VGLUT2 to excitatory neurons, and VGAT to inhibitory neurons, we injected a Cre-dependent viral vector to drive Chr2 in the vPAG of VGLUT2-Cre and VGAT-Cre mice. In VGLUT2-Cre mice, we observed robust oEPSCs at  $-60$  mV, with no response at 0 mV, in 100% of LC neurons recorded from (Figures 5A–5D). As expected, these oEPSCs were blocked by TTX, and rescued by 4-AP in the presence of TTX, as well as blocked by DNQX (Figures 5E and 5F). When comparing oEPSCs between VGLUT2-Cre and GAD2-Cre mice, oEPSCs in VGLUT2-Cre mice were significantly greater in amplitude than those from GAD2-Cre mice ( $p = 0.046$ ), likely reflecting that driving Chr2 into VGLUT2+ afferents captures a larger number of excitatory vPAG to LC afferents than GAD2+ vPAG afferents. This is consistent with our *in situ* hybridization findings of many VGLUT2+/GAD2-neurons (Figures 4 and S5A).

Conversely, in VGAT-Cre mice, oIPSCs were observed at 0 mV, with no response at  $-60$  mV in any neuron recorded from (Figures 5G–5J). Expression of YFP in the LC was lower than that present in VGLUT2-Cre mice, consistent with excitatory projections dominating vPAG to LC communication (Figures 5B and 5H). These oIPSCs were blocked by TTX, rescued by 4-AP, and blocked by Bicuculline (Figures 5K and 5L). Comparison of oIPSC amplitude between VGAT-Cre and GAD2-Cre mice yielded no significant differences ( $p = 0.187$ ), indicating that both promoters are likely targeting a similar quantity of vPAG inhibitory neurons (Figure S5B).

Overall, these findings support the existence of GAD2+/VGLUT2+ vPAG neurons that project to the LC, but are purely excitatory, and confirm that the use of VGLUT2-Cre and VGAT-Cre mice will provide means to selectively drive expression in exclusively excitatory and inhibitory neurons, respectively. To test our final hypothesis that this population of neurons might potentially release GABA in pathological conditions linked to chronic pain, we performed recordings of LC neurons from VGLUT2-Cre mice expressing Chr2 in excitatory vPAG neurons from both sham and nerve-injured mice. On day 14–18 after surgery, we found no evidence for a phenotypic switch, with 100% of recorded neurons possessing only oEPSCs, but no oIPSCs, and furthermore no change in oEPSC amplitude (Figure S6).

**DISCUSSION**

The use of Cre-recombinase to drive expression of fluorescent proteins and/or optical tools has proved an invaluable resource to neuroscience. However, caution is warranted with respect to the selectivity of promoters to specific populations of neurons. In this study, while using GAD2-Cre mouse lines to probe a potential functional inhibitory projection from the vPAG to LC, we unexpectedly found that GAD2 is also present in a population of VGLUT2+ vPAG neurons. Characterization through combined *in vitro* optogenetics and electrophysiology, immunohistochemistry, and *in situ* hybridization revealed this population to be VGLUT2+, CaMKII+, GAD2+, and GABA+, but VGAT-. Supporting this, we found no evidence that any VGLUT2+ vPAG neurons can support vesicular release of GABA, and conversely no VGAT+ vPAG neurons release glutamate. Therefore, this intersectional population of vPAG neurons is exclusively excitatory in terms of synaptic release, despite the presence of GAD2 and GABA.

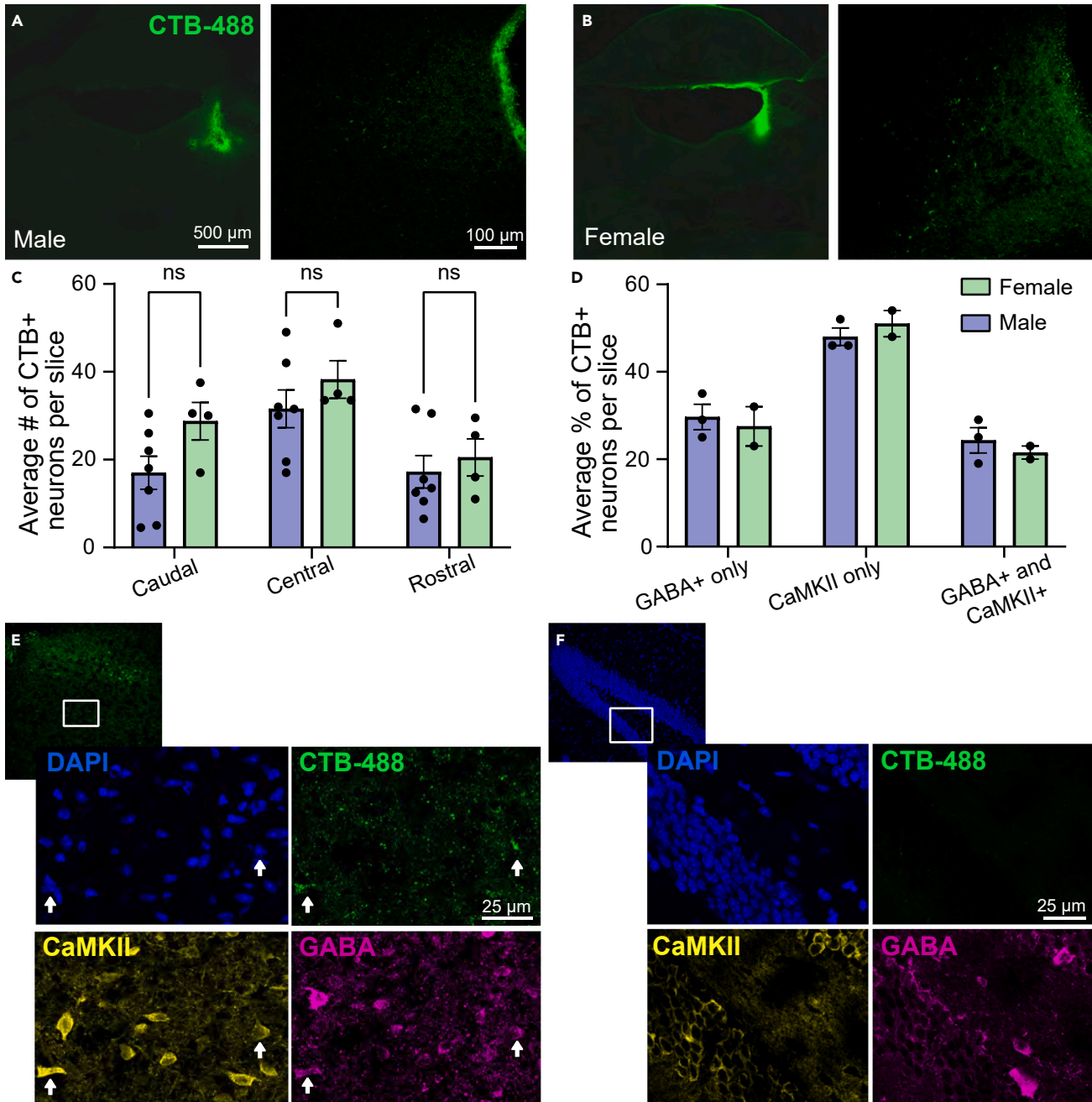


**Figure 3. Colocalization of GABA and CaMKII is present in vPAG to LC projecting neurons in both male and female mice**

(A and B) Low magnification images showing similar LC injection location (left) and vPAG distribution (right) of CTB+ neurons between male (A) and female (B) mice.

(C) Comparison of average number of CTB+ neurons in the vPAG after LC injection of CTB-488 in male and female mice (two-way ANOVA, location  $p = 0.003$ , sex  $p = 0.150$ , Sidak's post-hoc comparisons) (Male  $N = 921$  neurons from 42 slices/7 mice, Female  $N = 700$  neurons from 20 slices/4 mice).

(D) Average % of CTB+ neurons expressing GABA only, CaMKII only, or GABA and CaMKII (Male:  $N = 222$  neurons from 18 slices/3 mice, Female:  $N = 237$  neurons from 12 slices/2 mice).

(E) Representative image of immunohistochemical staining of vPAG neurons. Arrows indicate CTB488+ neurons expressing both CaMKII and GABA.

(F) Comparative image of immunohistochemical staining in the dentate gyrus showing separation of CaMKII and GABA signal. All error bars denote S.E.M.

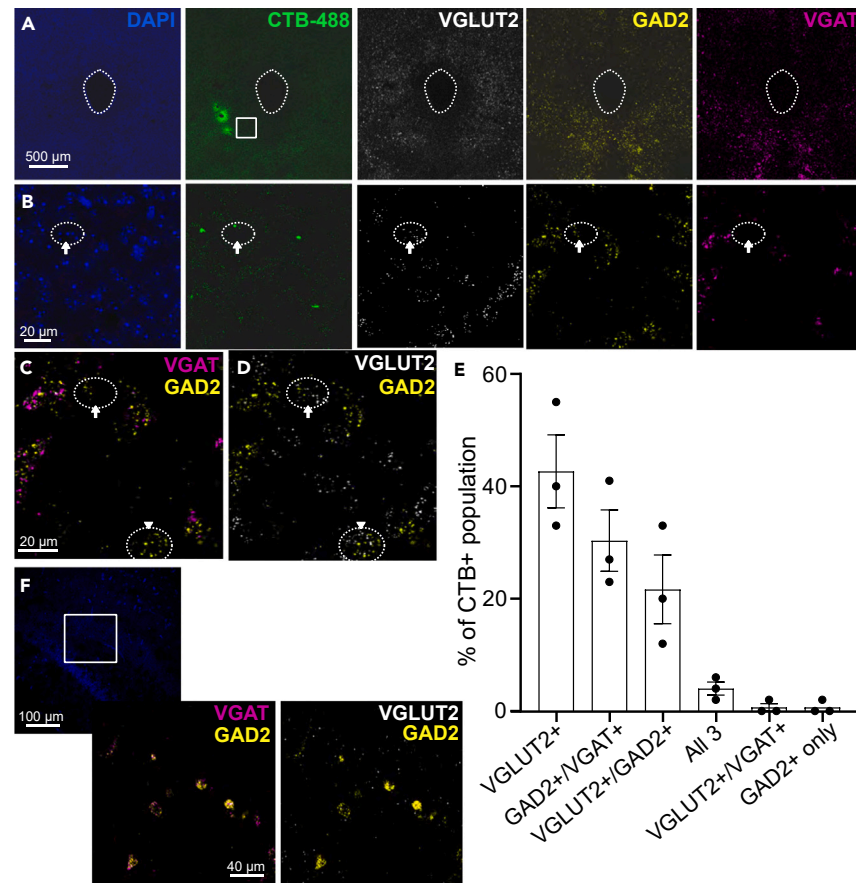


**Figure 4. RNAscope of vPAG to LC projecting neurons reveals a subpopulation of neurons that express both GAD2 and VGLUT2, but not VGAT**

(A) Low magnification images showing dorsoventral distribution of CTB-488 and mRNA for VGLUT2 (white), GAD2 (yellow), and VGAT (magenta) in the vPAG (delineated by dashed oval).  
 (B) Magnification of vPAG area in white rectangle in (A). Arrow represents a neuron expressing mRNA for both VGLUT2 and GAD2, but not VGAT.  
 (C) Merge of VGAT and GAD2 channels from (B) showing both CTB-488+ (arrow and dashed circle) and CTB-488- neurons (arrowhead and dashed circle) positive for GAD2 but negative for VGAT.  
 (D) Merge of VGLUT2 and GAD2 channels from (B) showing both CTB-488+ (arrow and dashed circle) and CTB-488- neurons (arrowhead and dashed circle) negative for VGAT but positive for VGLUT2.  
 (E) Quantification of relative % of the CTB+ neuron population positivity for VGLUT2, GAD2, and/or VGAT mRNA ( $N = 143$  neurons from 12 slices/3 mice).  
 (F) RNAscope in the dentate gyrus, with magnification of the area in the white rectangle showing no overlap of VGLUT2 and GAD2 signal. All error bars denote S.E.M.

The existence of this intersectional population of excitatory vPAG neurons which contain GAD2 and produce GABA was particularly interesting as we could find no evidence for synaptic GABA release. A similar population of neurons has previously been identified in the lateral habenula, where there was no evidence for GABA release despite the expression of GAD2.<sup>20</sup> It is possible that these neurons release GABA through reversal of GABA transporters such as GAT1, thereby bypassing the need for VGAT to release GABA into the extracellular space.<sup>29–31</sup> However, the existence of non-vesicular GABA release in this manner is contentious: while it appears possible for GAT1 to reverse transport if the membrane potential is sufficiently depolarized,<sup>29</sup> this seems unlikely in physiological conditions where extracellular GABA would be present due to nearby synaptic GABA release.<sup>32</sup>

Another possibility is that these neurons contain GAD2 and produce GABA such that they are ready to begin to release it in pathological conditions. This could be of particular interest given the importance of inhibitory tone in regulating behavioral output from both the vPAG and LC.<sup>6,33–35</sup> To test this possibility, we recorded from mice with the spared nerve injury (SNI) model of neuropathic pain but found no evidence that this excitatory population of neurons began to release GABA through vesicular means, at least to LC neurons. Although *de novo* expression of VGAT and release of GABA has not been reported in neurons that co-release GABA and glutamate, chronic conditions such as depression change the ratio of GABA to glutamate release.<sup>17</sup> However, it remains to be seen if there are any pathological conditions which could trigger VGAT expression and subsequent GABA and glutamate co-release in these vPAG neurons.

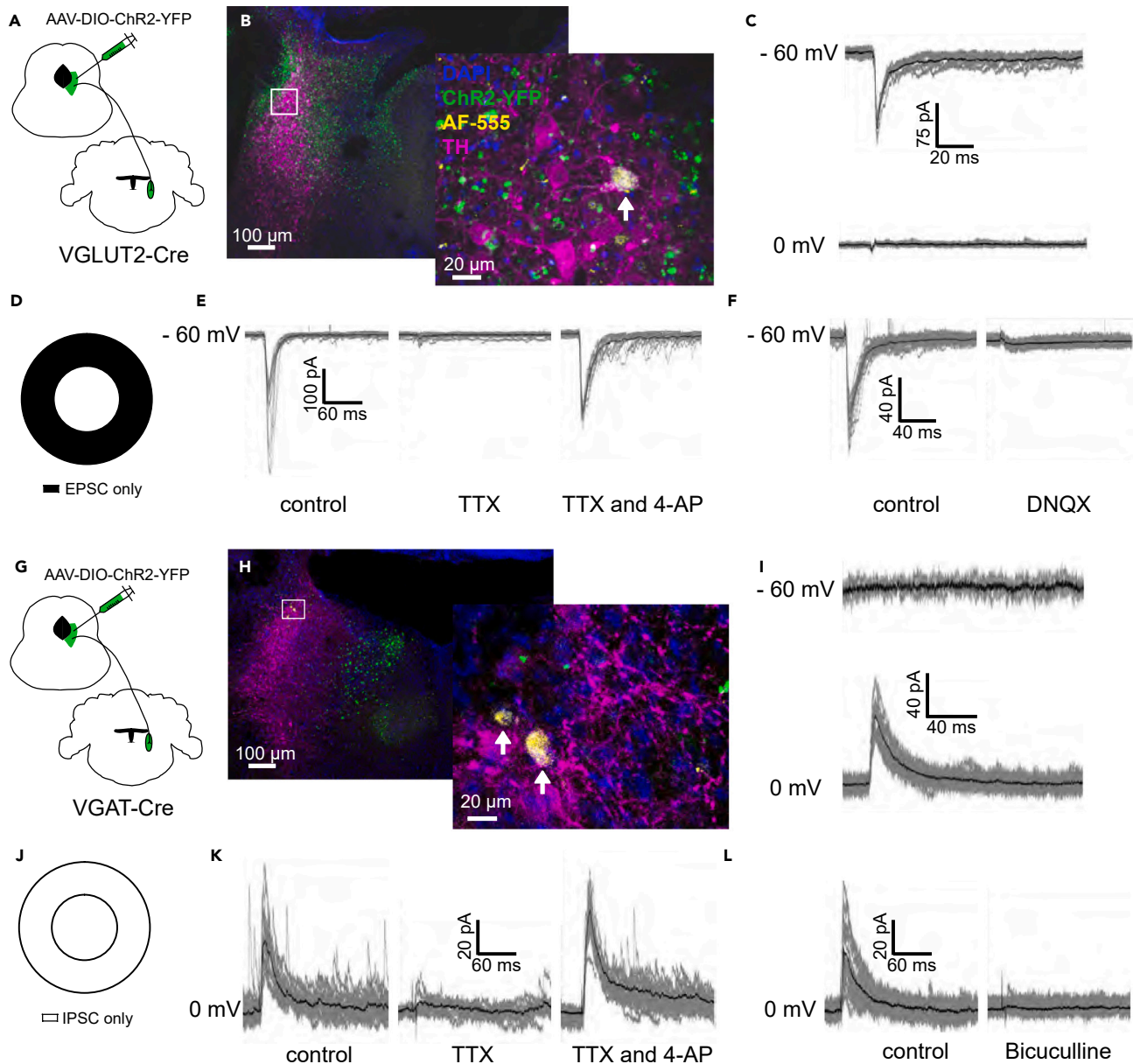


**Figure 5. Optogenetic stimulation of VGLUT2+ and VGAT+ afferents from the vPAG yields exclusively excitatory or inhibitory postsynaptic responses in LC neurons**

(A) Schematic of electrophysiological recording paradigm in VGLUT2-cre mice.

(B) Post-hoc immunohistochemistry confirming TH + identity of recorded locus coeruleus (LC) neuron.

(C and D) Optical stimulation of vPAG afferents yielded only EPSCs in 28 recorded LC neurons (3 mice, 28 LC neurons recorded in total).

(E) Representative trace of optically evoked EPSCs, demonstrating block of response by TTX and rescue by TTX + 4-AP perfusion. (F) Representative trace demonstrating block by DNQX.

(G) Schematic of electrophysiological recording paradigm in VGAT-cre mice.

(H) Post-hoc immunohistochemistry of recorded neurons.

(I and J) Optical stimulation of vPAG afferents yielded only IPSCs in 18 recorded LC neurons (7 mice, 32 LC neurons recorded in total).

(K) Representative trace of optically evoked IPSCs, with block by TTX and rescue by TTX + 4-AP.

(L) optically evoked IPSCs were fully blocked by Bicuculline.

A final possibility is that the presence of GAD2 and subsequent production of GABA in these vPAG neurons is a developmental holdover. This could be due to GABAergic synapses being earlier to develop embryonically, as well as the well-known GABA switch from excitation to inhibition as the internal chloride concentration decreases with increasing KCC2 expression in the early postnatal period.<sup>36–38</sup> In this way, early

GABAergic signaling in neuronal networks is proposed to promote proper circuit formation.<sup>36,39</sup> For example, granule cells of the dentate gyrus are excitatory in adult tissue but may express GAD1 and release GABA during differentiation and in juvenile tissue.<sup>40,41</sup> This could be tested in the vPAG by investigating the existence of this intersectional neuronal population along the developmental axis and characterizing the presence or absence of excitatory and inhibitory release in these neurons at various key time points during development.

GABAergic neurons have been well characterized in the PAG, with ample evidence for their role in modulating pain signaling such to produce analgesia, most notably through a characteristic action of opioids to inhibit vPAG GABA neurons that project to the RVM, thus providing disinhibition of descending signaling.<sup>33,35,42–44</sup> GABAergic neurons in the vPAG are also involved in anxiety and fear learning,<sup>28,45–47</sup> regulation of sleep and arousal,<sup>6,48,49</sup> prey hunting,<sup>50</sup> and feeding behaviors.<sup>51</sup> Importantly, opposing roles of GABAergic PAG neurons have been described in these latter two studies. The former reported that activation of GABA cells in the lateral PAG triggers increased food seeking whereas the latter study showed the opposite effect upon stimulation of the vPAG. This could in principle be due to the existence of different sub-populations of GABA cells in different parts of the PAG with distinct downstream projections. It is important to note, however that the former study utilized VGAT-Cre mice, whereas the latter relies on GAD2-Cre animals, and therefore it is possible that these authors may have activated GAD2 expressing glutamatergic cells, thus underscoring the importance of our present findings. Finally, while projections to the LC from the vPAG have been noted,<sup>4,8,52–55</sup> the potential of vPAG GABAergic neurons to project downstream to areas such as the LC is not well understood.<sup>10</sup>

Additionally, in this study we have demonstrated conclusively the existence of direct GABAergic innervation of noradrenergic neurons of the LC. First, *in situ* hybridization of the vPAG of mice injected with CTB-488 in the LC defined a significant population of CTB-488+ neurons that were also VGAT+ and GAD2+. Second, *in vitro* optogenetic activation of VGAT+ afferents from the vPAG while recording from identified TH+ neurons in the LC revealed monosynaptic optically evoked IPSCs, which were blocked by Bicuculline. Although these currents were not present in every neuron, they were present in 18/32 LC neurons recorded. Therefore, while excitatory drive from the vPAG to LC dominates, inhibitory drive into the LC represents about 25% of all projections.

Given the pronociceptive role of glutamatergic vPAG to LC projections,<sup>4</sup> it is tempting to speculate that GABAergic projections from the vPAG to LC may be antinociceptive. However, it is important to note that the LC contains a highly heterogeneous population of neurons, with projections to nearly every part of the central nervous system,<sup>2,56</sup> and an involvement in most aspects of arousal ranging from fear and pain to learning and wakefulness.<sup>56,57</sup> Indeed, activation of spinally projecting LC neurons produces analgesia, whereas activation of prefrontal cortex projecting neurons is highly anxiety-inducing.<sup>58</sup> Furthermore, there is evidence that the LC has a highly complex role in regulation of analgesia, as there is speculation that the LC may in fact drive chronic pain symptoms.<sup>59,60</sup> Understanding the relative roles of excitatory and inhibitory drive from the vPAG to LC, especially in the context of descending modulation of pain will be an interesting and important future area of study.

In summary, our data reveal functional inhibitory connections between the vPAG and the LC, and importantly, the existence of excitatory neuronal projections between these two brain regions that express the classical inhibitory neuronal marker GAD2. Caution is warranted when studying the role of this particular connection using a GAD2-Cre line to drive expression of optical tools such as ChR2 or GCaMP. Conceivably, by driving ChR2 into all GAD2+ neurons in the vPAG and then measuring behavioral output, the behavior observed would result from excitation of VGLUT2+/GAD2+ neurons. This would then represent simultaneous inhibition and excitation of the vPAG. We therefore recommend that future studies utilize the VGAT-Cre transgenic line when studying inhibitory projections from the vPAG, which does not appear to label any intersecting populations of vPAG neurons.

### Limitations of the study

A key limitation of our study is that we were unable to identify a specific biological role of GABA and glutamate coexpressing projection neurons. As noted above, our data indicate that there is no synaptic co-release of GABA and glutamate from nerve terminals in the LC in either naive or sciatic nerve-injured mice with neuropathic pain. We also examined the possibility of non-vesicular release of GABA from GAD2 expressing excitatory neurons within the vPAG, but were unable to detect such a phenomenon. Hence, it remains unclear whether GABA expressing glutamatergic neurons fulfill a specific physiological role, whether in naive or pathological conditions. Moreover, we acknowledge that our experiments were conducted exclusively in mice and it remains to be seen if our observations hold true for rats.

### STAR★METHODS

Detailed methods are provided in the online version of this paper and include the following:

- KEY RESOURCES TABLE
- RESOURCE AVAILABILITY
  - Lead contact
  - Materials availability
  - Data and code availability
- EXPERIMENTAL MODEL AND STUDY PARTICIPANT DETAILS
- METHOD DETAILS
  - Stereotaxic injections
  - Preparation of brainstem slices

- Optogenetics and electrophysiology
- Immunohistochemistry
- RNAscope *in situ* hybridization (ISH)
- **QUANTIFICATION AND STATISTICAL ANALYSIS**

## SUPPLEMENTAL INFORMATION

Supplemental information can be found online at <https://doi.org/10.1016/j.isci.2024.109972>.

## ACKNOWLEDGMENTS

G.W.Z. is supported by grants from the Canadian Institutes of Health Research (CIHR) and holds a Canada Research Chair. T.T. is supported by grants from the Canadian Institutes of Health Research and Natural Sciences and Engineering Research Council of Canada. E.K.H. is supported by an Eyes High postdoctoral fellowship, a Spinal Cord Nerve Injury and Pain postdoctoral fellowship, and a CIHR postdoctoral fellowship. J.C.-P. is supported by a Spinal Cord Nerve Injury and Pain postdoctoral fellowship. We thank Lina Chen for processing brain tissue slices for RNAscope experiments.

## AUTHOR CONTRIBUTIONS

E.K.H., Z.Z., and G.W.Z. conceived the study, G.W.Z. and T.T. supervised the work. Z.Z. performed all stereotaxic injections, Z.Z. and E.K.H. performed electrophysiological experiments. E.K.H. and S.S.-H. performed all immunohistochemical staining, confocal imaging, and image counting and analysis, J.C.-P. and S.S.-H. performed RNAscope experiments. E.K.H. and Z.Z. wrote the manuscript. All authors contributed to editing of the manuscript.

## DECLARATION OF INTERESTS

The authors declare no competing interests.

Received: December 1, 2023

Revised: January 12, 2024

Accepted: May 10, 2024

Published: May 16, 2024

## REFERENCES

1. George, D.T., Ameli, R., and Koob, G.F. (2019). Periaqueductal Gray Sheds Light on Dark Areas of Psychopathology. *Trends Neurosci.* *42*, 349–360. <https://doi.org/10.1016/j.tins.2019.03.004>.
2. Breton-Provencher, V., Drummond, G.T., and Sur, M. (2021). Locus Coeruleus Norepinephrine in Learned Behavior: Anatomical Modularity and Spatiotemporal Integration in Targets. *Front. Neural Circuits* *15*, 638007. <https://doi.org/10.3389/fncir.2021.638007>.
3. Benarroch, E.E. (2012). Periaqueductal gray: An interface for behavioral control. *Neurology* *78*, 210–217. <https://doi.org/10.1212/WNL.0b013e31823fcdde>.
4. Kim, J.H., Gangadharan, G., Byun, J., Choi, E.J., Lee, C.J., and Shin, H.S. (2018). Yin-and-yang bifurcation of opioidergic circuits for descending analgesia at the midbrain of the mouse. *Proc. Natl. Acad. Sci. USA* *115*, 11078–11083. <https://doi.org/10.1073/pnas.1806082115>.
5. Schwarz, L.A., and Luo, L. (2015). Organization of the locus coeruleus-norepinephrine system. *Curr. Biol.* *25*, R1051–R1056. <https://doi.org/10.1016/j.cub.2015.09.039>.
6. Weber, F., Hoang Do, J.P., Chung, S., Beier, K.T., Bikov, M., Saffari Doost, M., and Dan, Y. (2018). Regulation of REM and Non-REM Sleep by Periaqueductal GABAergic Neurons. *Nat. Commun.* *9*, 354. <https://doi.org/10.1038/s41467-017-02765-w>.
7. Ennis, M., Behbehani, M., Shipley, M.T., van Bockstaele, E.J., and Aston-Jones, G. (1991). Projections from the periaqueductal gray to the rostromedial pericoerulear region and nucleus locus coeruleus: Anatomic and physiologic studies. *J. Comp. Neurol.* *306*, 480–494. <https://doi.org/10.1002/cne.903060311>.
8. Van Bockstaele, E.J., Bajic, D., Proudfit, H., and Valentino, R.J. (2001). Topographic architecture of stress-related pathways targeting the noradrenergic locus coeruleus. *Physiol. Behav.* *73*, 273–283. [https://doi.org/10.1016/S0031-9384\(01\)00448-6](https://doi.org/10.1016/S0031-9384(01)00448-6).
9. Aston-Jones, G., Shipley, M.T., Chouvet, G., Ennis, M., van Bockstaele, E., Pieribone, V., Shiekhhattar, R., Akaoka, H., Drolet, G., Astier, B., et al. (1991). Afferent regulation of locus coeruleus neurons: Anatomy, physiology and pharmacology. *Prog. Brain Res.* *88*, 47–75. [https://doi.org/10.1016/S0079-6123\(08\)63799-1](https://doi.org/10.1016/S0079-6123(08)63799-1).
10. Huang, J., Gadotti, V.M., Chen, L., Souza, I.A., Huang, S., Wang, D., Ramakrishnan, C., Deisseroth, K., Zhang, Z., and Zamponi, G.W. (2019). A neuronal circuit for activating descending modulation of neuropathic pain. *Nat. Neurosci.* *22*, 1659–1668. <https://doi.org/10.1038/s41593-019-0481-5>.
11. Soghomonian, J.J., and Martin, D.L. (1998). Two isoforms of glutamate decarboxylase: Why? *Trends Pharmacol. Sci.* *19*, 500–505. [https://doi.org/10.1016/S0165-6147\(98\)01270-X](https://doi.org/10.1016/S0165-6147(98)01270-X).
12. Feldblum, S., Erlander, M.G., and Tobin, A.J. (1993). Different distributions of GAD65 and GAD67 mRNAs suggest that the two glutamate decarboxylases play distinctive functional roles. *J. Neurosci. Res.* *34*, 689–706. <https://doi.org/10.1002/jnr.490340612>.
13. McIntire, S.L., Reimer, R.J., Schuske, K., Edwards, R.H., and Jorgensen, E.M. (1997). Identification and characterization of the vesicular GABA transporter. *Nature* *389*, 870–876. <https://doi.org/10.1038/39908>.
14. Taniguchi, H., He, M., Wu, P., Kim, S., Paik, R., Sugino, K., Kvitsiani, D., Fu, Y., Lu, J., Lin, Y., et al. (2011). A Resource of Cre Driver Lines for Genetic Targeting of GABAergic Neurons in Cerebral Cortex. *Neuron* *71*, 995–1013. <https://doi.org/10.1016/j.neuron.2011.07.026>.
15. Nguyen, A.Q., Dela Cruz, J.A.D., Sun, Y., Holmes, T.C., and Xu, X. (2016). Genetic cell targeting uncovers specific neuronal types and distinct subregions in the bed nucleus of the stria terminalis. *J. Comp. Neurol.* *524*, 2379–2399. <https://doi.org/10.1002/cne.23954>.
16. Tritsch, N.X., Granger, A.J., and Sabatini, B.L. (2016). Mechanisms and functions of GABA co-release. *Nat. Rev. Neurosci.* *17*, 139–145. <https://doi.org/10.1038/nrn.2015.21>.
17. Shabel, S.J., Proulx, C.D., Piriz, J., and Malinow, R. (2014). GABA/glutamate co-release controls habenula output and is modified by antidepressant treatment.

- Science 345, 1494–1498. <https://doi.org/10.1126/science.1250469>.
18. Yoo, J.H., Zell, V., Gutierrez-Reed, N., Wu, J., Ressler, R., Shenasa, M.A., Johnson, A.B., Fife, K.H., Faget, L., and Hnasko, T.S. (2016). Ventral tegmental area glutamate neurons co-release GABA and promote positive reinforcement. *Nat. Commun.* 7, 13697. <https://doi.org/10.1038/ncomms13697>.
  19. Seal, R.P., and Edwards, R.H. (2006). Functional implications of neurotransmitter co-release: Glutamate and GABA share the load. *Curr. Opin. Pharmacol.* 6, 114–119. <https://doi.org/10.1016/j.coph.2005.12.001>.
  20. Quina, L.A., Walker, A., Morton, G., Han, V., and Turner, E.E. (2020). GAD2 expression defines a class of excitatory lateral habenula neurons in mice that project to the raphe and pontine tegmentum. *eNeuro* 7. <https://doi.org/10.1523/ENEURO.0527-19.2020>.
  21. Moffitt, J.R., Bambah-Mukku, D., Eichhorn, S.W., Vaughn, E., Shekhar, K., Perez, J.D., Rubinstein, N.D., Hao, J., Regeve, A., Dulac, C., and Zhuang, X. (2018). Molecular, spatial, and functional single-cell profiling of the hypothalamic preoptic region. *Science* 362, eaau5324. <https://doi.org/10.1126/science.aau5324>.
  22. Kosse, C., Schöne, C., Bracey, E., and Burdakov, D. (2017). Orexin-driven GAD65 network of the lateral hypothalamus sets physical activity in mice. *Proc. Natl. Acad. Sci. USA* 114, 4525–4530. <https://doi.org/10.1073/pnas.1619700114>.
  23. Keaveney, M.K., Rahsepar, B., Tseng, H.A., Fernandez, F.R., Mount, R.A., Ta, T., White, J.A., Berg, J., and Han, X. (2020). CaMKII $\alpha$ -positive interneurons identified via a microRNA-based viral gene targeting strategy. *J. Neurosci.* 40, 9576–9588. <https://doi.org/10.1523/JNEUROSCI.2570-19.2020>.
  24. Larsson, M. (2018). Non-canonical heterogeneous cellular distribution and colocalization of CaMKII $\alpha$  and CaMKII $\beta$  in the spinal superficial dorsal horn. *Brain Struct. Funct.* 223, 1437–1457. <https://doi.org/10.1007/s00429-017-1566-0>.
  25. Yasuda, R., Hayashi, Y., and Hell, J.W. (2022). CaMKII: a central molecular organizer of synaptic plasticity, learning and memory. *Nat. Rev. Neurosci.* 23, 666–682. <https://doi.org/10.1038/s41583-022-00624-2>.
  26. Loyd, D.R., and Murphy, A.Z. (2006). Sex differences in the anatomical and functional organization of the periaqueductal gray-rostral ventromedial medullary pathway in the rat: A potential circuit mediating the sexually dimorphic actions of morphine. *J. Comp. Neurol.* 496, 723–738. <https://doi.org/10.1002/cne.20962>.
  27. Yu, W., Pati, D., Pina, M.M., Schmidt, K.T., Boyt, K.M., Hunker, A.C., Zweifel, L.S., McElligott, Z.A., and Kash, T.L. (2021). Periaqueductal gray/dorsal raphe dopamine neurons contribute to sex differences in pain-related behaviors. *Neuron* 109, 1365–1380.e5. <https://doi.org/10.1016/j.neuron.2021.03.001>.
  28. Llorente-Berzal, A., McGowan, F., Gaspar, J.C., Rea, K., Roche, M., and Finn, D.P. (2022). Sexually Dimorphic Expression of Fear-conditioned Analgesia in Rats and Associated Alterations in the Endocannabinoid System in the Periaqueductal Grey. *Neuroscience* 480, 117–130. <https://doi.org/10.1016/j.neuroscience.2021.11.005>.
  29. Wu, Y., Wang, W., Diez-Sampedro, A., and Richerson, G.B. (2007). Nonvesicular Inhibitory Neurotransmission via Reversal of the GABA Transporter GAT-1. *Neuron* 56, 851–865. <https://doi.org/10.1016/j.neuron.2007.10.021>.
  30. Koch, U., and Magnusson, A.K. (2009). Unconventional GABA release: mechanisms and function. *Curr. Opin. Neurobiol.* 19, 305–310. <https://doi.org/10.1016/j.conb.2009.03.006>.
  31. Bertram, S., Cherubino, F., Bossi, E., Castagna, M., and Peres, A. (2011). GABA reverse transport by the neuronal cotransporter GAT1: Influence of internal chloride depletion. *Am. J. Physiol. Cell Physiol.* 301, C1064–C1073. <https://doi.org/10.1152/ajpcell.00120.2011>.
  32. Savtchenko, L., Megalogeni, M., Rusakov, D.A., Walker, M.C., and Pavlov, I. (2015). Synaptic GABA release prevents GABA transporter type-1 reversal during excessive network activity. *Nat. Commun.* 6, 6597. <https://doi.org/10.1038/ncomms7597>.
  33. Xie, L., Wu, H., Chen, Q., Xu, F., Li, H., Xu, Q., Jiao, C., Sun, L., Ullah, R., and Chen, X. (2023). Divergent modulation of pain and anxiety by GABAergic neurons in the ventrolateral periaqueductal gray and dorsal raphe. *Neuropsychopharmacology* 48, 1509–1519. <https://doi.org/10.1038/s41386-022-01520-0>.
  34. Breton-Provencher, V., and Sur, M. (2019). Active control of arousal by a locus coeruleus GABAergic circuit. *Nat. Neurosci.* 22, 218–228. <https://doi.org/10.1038/s41593-018-0305-z>.
  35. Samineneni, V.K., Grajales-Reyes, J.G., Copits, B.A., O'Brien, D.E., Trigg, S.L., Gomez, A.M., Bruchas, M.R., and Gereau, R.W. (2017). Divergent modulation of nociception by glutamatergic and GABAergic neuronal subpopulations in the periaqueductal gray. *eNeuro* 4. <https://doi.org/10.1523/ENEURO.0129-16.2017>.
  36. Owens, D.F., and Kriegstein, A.R. (2002). Is there more to GABA than synaptic inhibition? *Nat. Rev. Neurosci.* 3, 715–727. <https://doi.org/10.1038/nrn919>.
  37. Ben-Ari, Y. (2002). Excitatory actions of GABA during development: The nature of the nurture. *Nat. Rev. Neurosci.* 3, 728–739. <https://doi.org/10.1038/nrn920>.
  38. Ganguly, K., Schinder, A.F., Wong, S.T., and Poo, M. (2001). GABA itself promotes the developmental switch of neuronal GABAergic responses from excitation to inhibition. *Cell* 105, 521–532. [https://doi.org/10.1016/S0092-8674\(01\)00341-5](https://doi.org/10.1016/S0092-8674(01)00341-5).
  39. Wang, D.D., and Kriegstein, A.R. (2009). Defining the role of GABA in cortical development. *J. Physiol.* 587, 1873–1879. <https://doi.org/10.1113/jphysiol.2008.167635>.
  40. Cabezas, C., Irinopoulou, T., Cauli, B., and Ponce, J.C. (2013). Molecular and functional characterization of GAD67-expressing, newborn granule cells in mouse dentate gyrus. *Front. Neural Circuits* 7, 60. <https://doi.org/10.3389/fncir.2013.00060>.
  41. Gutiérrez, R., Romo-Parra, H., Maqueda, J., Vivar, C., Ramírez, M., Morales, M.A., and Lamas, M. (2003). Plasticity of the GABAergic phenotype of the “glutamatergic” granule cells of the rat dentate gyrus. *J. Neurosci.* 23, 5594–5598. <https://doi.org/10.1523/jneurosci.23-13-05594.2003>.
  42. Park, C., Kim, J.H., Yoon, B.E., Choi, E.J., Lee, C.J., and Shin, H.S. (2010). T-type channels control the opioidergic descending analgesia at the low threshold-spiking GABAergic neurons in the periaqueductal gray. *Proc. Natl. Acad. Sci. USA* 107, 14857–14862. <https://doi.org/10.1073/pnas.1009532107>.
  43. Tonsfeldt, K.J., Suchland, K.L., Beeson, K.A., Lowe, J.D., Li, M.H., and Ingram, S.L. (2016). Sex differences in GABA signaling in the periaqueductal gray induced by persistent inflammation. *J. Neurosci.* 36, 1669–1681. <https://doi.org/10.1523/JNEUROSCI.1928-15.2016>.
  44. Fields, H. (2004). State-dependent opioid control of pain. *Nat. Rev. Neurosci.* 5, 565–575. <https://doi.org/10.1038/nrn1431>.
  45. Hon, O.J., DiBerto, J.F., Mazzone, C.M., Sugam, J., Bloodgood, D.W., Hardaway, J.A., Husain, M., Kendra, A., McCall, N.M., Lopez, A.J., et al. (2022). Serotonin modulates an inhibitory input to the central amygdala from the ventral periaqueductal gray. *Neuropsychopharmacology* 47, 2194–2204. <https://doi.org/10.1038/s41386-022-01392-4>.
  46. Lowery-Gionta, E.G., DiBerto, J., Mazzone, C.M., and Kash, T.L. (2018). GABA neurons of the ventral periaqueductal gray area modulate behaviors associated with anxiety and conditioned fear. *Brain Struct. Funct.* 223, 3787–3799. <https://doi.org/10.1007/s00429-018-1724-z>.
  47. Rea, K., Lang, Y., and Finn, D.P. (2009). Alterations in Extracellular Levels of Gamma-Aminobutyric Acid in the Rat Basolateral Amygdala and Periaqueductal Gray During Conditioned Fear, Persistent Pain and Fear-Conditioned Analgesia. *J. Pain* 10, 1088–1098. <https://doi.org/10.1016/j.jpain.2009.04.019>.
  48. Guo, Y., Song, Y., Cao, F., Li, A., Hao, X., Shi, W., Zhou, Z., Cao, J., Liu, Y., Mi, W., and Tong, L. (2023). Ventrolateral periaqueductal gray GABAergic neurons promote arousal of sevoflurane anesthesia through cortico-midbrain circuit. *iScience* 26, 107486. <https://doi.org/10.1016/j.isci.2023.107486>.
  49. Lu, J., Sherman, D., Devor, M., and Saper, C.B. (2006). A putative flip-flop switch for control of REM sleep. *Nature* 441, 589–594. <https://doi.org/10.1038/nature04767>.
  50. Yu, H., Xiang, X., Chen, Z., Wang, X., Dai, J., Wang, X., Huang, P., Zhao, Z.D., Shen, W.L., and Li, H. (2021). Periaqueductal gray neurons encode the sequential motor program in hunting behavior of mice. *Nat. Commun.* 12, 6523. <https://doi.org/10.1038/s41467-021-26852-1>.
  51. Hao, S., Yang, H., Wang, X., He, Y., Xu, H., Wu, X., Pan, L., Liu, Y., Lou, H., Xu, H., et al. (2019). The Lateral Hypothalamic and BNST GABAergic Projections to the Anterior Ventrolateral Periaqueductal Gray Regulate Feeding. *Cell Rep.* 28, 616–624.e5. <https://doi.org/10.1016/j.celrep.2019.06.051>.
  52. Fan, X., Song, J., Ma, C., Lv, Y., Wang, F., Ma, L., and Liu, X. (2022). Noradrenergic signaling mediates cortical early tagging and storage of remote memory. *Nat. Commun.* 13, 7623. <https://doi.org/10.1038/s41467-022-35342-x>.
  53. Proudfit, H.K. (2002). The challenge of defining brainstem pain modulation circuits. *J. Pain* 3, 350–359. <https://doi.org/10.1054/jpai.2002.127777>.
  54. Lubejko, S., Livrizzi, G., and Banghart, M.R. (2022). Investigating the Role of the Locus Coeruleus in Periaqueductal Gray-mediated Antinociception. *J. Pain* 23, 24. <https://doi.org/10.1016/j.jpain.2022.03.093>.
  55. Bajic, D., and Proudfit, H.K. (1999). Projections of neurons in the periaqueductal gray to pontine and medullary catecholamine cell groups involved in the modulation of nociception. *J. Comp. Neurol.* 405, 359–379.

- [https://doi.org/10.1002/\(SICI\)1096-9861\(19990315\)405:3<359::AID-CNE6>3.0.CO;2](https://doi.org/10.1002/(SICI)1096-9861(19990315)405:3<359::AID-CNE6>3.0.CO;2).
56. Poe, G.R., Foote, S., Eschenko, O., Johansen, J.P., Bouret, S., Aston-Jones, G., Harley, C.W., Manahan-Vaughan, D., Weinschenker, D., Valentino, R., et al. (2020). Locus coeruleus: a new look at the blue spot. *Nat. Rev. Neurosci.* *21*, 644–659. <https://doi.org/10.1038/s41583-020-0360-9>.
57. Aston-Jones, G., and Cohen, J.D. (2005). An integrative theory of locus coeruleus-norepinephrine function: Adaptive gain and optimal performance. *Annu. Rev. Neurosci.* *28*, 403–450. <https://doi.org/10.1146/annurev.neuro.28.061604.135709>.
58. Hirschberg, S., Li, Y., Randall, A., Kremer, E.J., and Pickering, A.E. (2017). Functional dichotomy in spinal- vs prefrontal-projecting locus coeruleus modules splits descending noradrenergic analgesia from ascending aversion and anxiety in rats. *Elife* *6*, e29808. <https://doi.org/10.7554/elife.29808>.
59. Taylor, B.K., and Westlund, K.N. (2017). The noradrenergic locus coeruleus as a chronic pain generator. *J. Neurosci. Res.* *95*, 1336–1346. <https://doi.org/10.1002/jnr.23956>.
60. Kucharczyk, M.W., Di Domenico, F., and Bannister, K. (2022). Distinct brainstem to spinal cord noradrenergic pathways inversely regulate spinal neuronal activity. *Brain* *145*, 2293–2300. <https://doi.org/10.1093/brain/awac085>.
61. Grabinski, T.M., Kneynsberg, A., Manfredsson, F.P., and Kanaan, N.M. (2015). A method for combining mrascope in situ hybridization with immunohistochemistry in thick free-floating brain sections and primary neuronal cultures. *PLoS One* *10*, e0120120. <https://doi.org/10.1371/journal.pone.0120120>.

## STAR★METHODS

## KEY RESOURCES TABLE

| REAGENT or RESOURCE   | SOURCE                   | IDENTIFIER                           |
|---|--------------------------|--------------------------------------|
| <b>Antibodies</b>   |                          |                                      |
| Sheep Anti-Tyrosine Hydroxylase Antibody, polyclonal          | EMD Millipore            | Cat#AB1542, RRID:AB_90755            |
| Mouse CaMKII alpha Monoclonal Antibody (6G9)                  | Thermo Fisher Scientific | Cat#MA1-048<br>RRID:AB_325403        |
| Rabbit Anti-GABA polyclonal antibody                          | Millipore Sigma          | Cat#A2052 RRID:AB_477652             |
| Donkey anti-Sheep IgG (H + L) Secondary Ab, 647               | Thermo Fisher Scientific | Cat#A21448<br>RRID:AB_2535865        |
| Donkey Anti-Mouse IgG H&L, 568                                | Abcam                    | Cat#ab175472<br>RRID:AB_2636996      |
| Donkey anti-Mouse IgG (H + L), Secondary Ab, 647              | Thermo Fisher Scientific | Cat#A31571<br>RRID:AB_162542         |
| Goat anti-Rabbit IgG F(ab') <sub>2</sub> Secondary Ab, FITC   | Thermo Fisher Scientific | Cat#A31573<br>RRID:AB_2536183        |
| <b>Bacterial and virus strains</b>                            |                          |                                      |
| AAV9-EF1 $\alpha$ -double floxed-Chr2 (H134R)-EYFP-WPRE-HGHpA | Addgene                  | Addgene #20298<br>RRID:Addgene_20298 |
| <b>Chemicals, peptides, and recombinant proteins</b>          |                          |                                      |
| Alexa Fluor 488 conjugate                                     | Thermo Fisher Scientific | Cat#C22841                           |
| TTX citrate   | Alomone                  | Cat#T-550                            |
| 4-AP (4-aminopyridine)  | Millipore Sigma          | Cat#A-0152                           |
| Bicuculline methochloride                                     | Tocris                   | Cat#0131/10                          |
| DNQX  | Tocris                   | Cat#0189/10                          |
| QX 314 chloride   | Tocris                   | Cat#2313/50                          |
| <b>Experimental models: Organisms/strains</b>                 |                          |                                      |
| Vglut2-ires-Cre mice: Strain #:016963                         | The Jackson lab          | RRID:IMSR_JAX:016963                 |
| Vgat-ires-Cre knock-in: Strain #:028862                       | The Jackson lab          | RRID:IMSR_JAX:02886                  |
| Gad2-ires-Cre: Strain #:010802                                | The Jackson lab          | RRID:IMSR_JAX:01080                  |
| Ai9 or Ai9(RCL-tdT): Strain #:007909                          | The Jackson lab          | RRID:IMSR_JAX:007909                 |
| <b>Oligonucleotides</b>                                       |                          |                                      |
| RNAscope Multiplex kit  | ACD a biotechnie brand   | Cat#323110                           |
| RNAscope™ Probe, Gad2   | ACD a biotechnie brand   | Cat#439371-C1                        |
| RNAscope™ Probe, Vgat, Slc17a6                                | ACD a biotechnie brand   | Cat#319171-C2                        |
| RNAscope™ Probe, Vglut2, Slc32a1                              | ACD a biotechnie brand   | Cat#319191-C3                        |
| RNAscope™ Positive Control against Polr2a, PPIB, and UBC      | ACD a biotechnie brand   | Cat#320881                           |
| RNAscope™ Negative Control against DapB                       | ACD a biotechnie brand   | Cat#320871                           |
| <b>Other</b>  |                          |                                      |
| H2O2  | ACD a biotechnie brand   | Cat#322381                           |

## RESOURCE AVAILABILITY

## Lead contact

Further information and requests for resources and reagents should be directed to and will be fulfilled by the lead contact, Dr. Gerald W. Zamponi ([zamponi@ucalgary.ca](mailto:zamponi@ucalgary.ca)).

### Materials availability

This study did not generate new unique reagents.

### Data and code availability

- Microscopy data reported in this paper will be shared by the [lead contact](#) upon request.
- This paper does not report original code.
- Any additional information required to reanalyze the data reported in this paper is available from the [lead contact](#) upon request.

## EXPERIMENTAL MODEL AND STUDY PARTICIPANT DETAILS

All experiments involving animals were approved by the University of Calgary Animal Care Committee. Mice were maintained on a 12 h light: dark cycle, with lights turning off at 7 p.m. All surgeries were performed during the light cycle, beginning after 9 a.m., and ending before 5 p.m. Food and water were available *ad libitum*. Experiments involved both male and female C57BL/6J adult wild-type and transgenic mice, all originally purchased from Jackson Laboratories. Four transgenic lines were used: VGLUT2-Cre: *Slc17a6<sup>tm2(cre)Lowl</sup>/J* (Jackson stock #: 016963), GAD2-Cre: *Gad2<sup>tm2(cre)Zjh</sup>/J* (Jackson stock #: 010802), Ai9: B6.Cg-Gt(ROSA)26Sor<sup>tm9(CAG-tdTomato)Hze</sup>/J (Jackson stock #: 007909), VGAT-Cre: B6J.129S6(FVB)-*Slc32a1<sup>tm2(cre)Lowl</sup>/MwarJ* (Jackson stock #: 028862). To produce VGLUT2-Cre x ai9 and GAD2-Cre x ai9, two female ai9 or Cre mice were bred in a harem with one male Cre or ai9 mouse in house. All littermates of the same sex were randomly assigned to experimental groups.

## METHOD DETAILS

### Stereotaxic injections

Male mice (8–10 weeks old, 24–29g) were anesthetized with isoflurane (4–5% for induction, 1.5–2.5% for maintenance) in a stereotaxic frame (Stoelting). Viral titers of adeno-associated virus (AAV) vectors were between  $2 \times 10E^{12}$  and  $9.9 \times 10E^{12}$  viral genomes per milliliter. To express Channelrhodopsin (ChR2) in the vPAG, AAV9-EF1 $\alpha$ -double floxed-ChR2 (H134R)-EYFP-WPRE-HGHpA (400–500 nL) (Addgene #20298), was injected using an automatic nanoliter injector (Nanoject II, Drummond Scientific) positioned into the right vPAG (anteroposterior (AP) –4.59 mm; right (R) –0.4 mm; dorsoventral (DV) –3.3 mm). To retrogradely trace the vPAG to LC projection, cholera toxin subunit B, Alexa Fluor 488 conjugate (0.1%, w/v, 400–500 nL, CTB-488, Thermo Fisher Scientific, #C22841) was injected into the right LC (AP –5.32 mm; R –0.75 mm; DV –4.00 mm). For some experiments, female C57BL/6J mice were used (8–12 weeks old, 17–22g), with modified coordinates for the right LC (AP: –5.30 mm; Right –0.73 mm; DV –3.90 mm).

Injections were performed using a digital stereotaxic frame with a glass capillary. The viral suspensions and CTB-488 were delivered at 50 nLx2/min (2 boluses/min). After completing the injection, the injection capillary remained in position for 5 min and then was raised 100  $\mu$ m with an additional 10 min wait to allow for the virus/CTB-488 to diffuse at the injection site, and then the glass needle was slowly withdrawn. Viruses were allowed to express for at least 8 weeks before optogenetic manipulation. CTB-488 was allowed to retrogradely travel into the vPAG for 3 weeks before perfusion. For projection tracing, the numbers of mice given in the figure captions reflect successful repetitions. A small number of mice were excluded from electrophysiology when ChR2 failed to evoke optically-induced inward current > 20 pA in more than four consecutive neurons. Likewise, a small number of mice were excluded from CTB-488 immunohistochemical analysis due to injection sites not aligning within 50  $\mu$ m of the LC.

### Preparation of brainstem slices

Brainstem slices were prepared for electrophysiology as previously described.<sup>10</sup> Adult (8–10 weeks) male mice (VGLUT2-Cre, GAD2-Cre, VGAT-Cre) were first injected with a viral vector to express ChR2 in vPAG neurons expressing Cre. 8–10 weeks later, mice were euthanized with an overdose of isoflurane and a transcardial perfusion was performed with ice-cold NMDG (N-methyl-D-glucamine) solution (in mM: NMDG 93, KCl 2.5, NaH<sub>2</sub>PO<sub>4</sub> 1.2, NaHCO<sub>3</sub> 30, HEPES 20, Glucose 25, Na-ascorbate 5, Na-pyruvate 3, CaCl<sub>2</sub>·2H<sub>2</sub>O 0.5, MgSO<sub>4</sub>·7H<sub>2</sub>O 10, Thiourea 2). Brains were then recovered, and the frontal half of the brain was discarded. They were then mounted frontal side down onto a vibratome chuck with superglue. Brains were sliced on a vibratome (Leica VT1200S, Leica Biosystems) in ice-cold NMDG solution bubbled with 95% O<sub>2</sub>/5% CO<sub>2</sub>. Vibratome settings were as follows: speed = 0.16 mm/s, amplitude = 1 mm, thickness of slice = 260  $\mu$ m. Slices containing LC were chosen based on shape of the fourth ventricle. Approximately 1–2 slices per mouse could be recovered that contained the LC. Slices were immediately removed from ice-cold NMDG solution and placed into a beaker filled with NMDG solution within a water bath at 34°C for 11 min. Immediately following this, slices were then moved into a beaker of ACSF (in mM: NaCl 120, NaH<sub>2</sub>PO<sub>4</sub> 1.25, NaHCO<sub>3</sub> 26, glucose 25, CaCl<sub>2</sub> 2.5, KCl 2.5, MgSO<sub>4</sub>·7H<sub>2</sub>O 1.3) for an additional 35 min at 34°C. Following this, slices were allowed to recover to room temperature prior to placing under a microscope for electrophysiology.

### Optogenetics and electrophysiology

Brainstem slices were placed under a Zeiss Axioexaminer (Axioskop 2) microscope for electrophysiology and held down with a steel harp. Slices were maintained at 31°C–33°C using an in-line heater (TC-324B, Warner Instruments) for 95% O<sub>2</sub>/5% CO<sub>2</sub> bubbled ACSF. ACSF was perfused through gravity perfusion at a rate of 2 mL/min. Voltage-clamp whole cell electrophysiology was performed on individual LC

neurons, confirmed through post-hoc immunohistochemistry as being TH<sup>+</sup>. Recording pipettes were pulled from glass capillaries (#BF150-86-7.5, Sutter Instruments) on a Zeitz DMZ Universal pipette puller, with end resistance of 4–5M $\Omega$ . Internal recording solution contained (in mM): CH<sub>3</sub>CO<sub>3</sub>S 130, CsCl 4, EGTA 2, ATP-Mg 4, GTP-Na 0.3, HEPES 10, QX-314 5, AF-555 0.05, pH 7.3.

Micromanipulators (MC1000E, Sutter Instruments) were used for the recording pipette and to hold the optic stimulation fiber, maintained on opposite sides of the holding chamber. Optic stimulation was provided through a 473 nm diode-pumped solid-state (DPSS) laser (Laserglow Technologies) equipped with a fibreoptic cannula (Thorlabs CFMC12L20, 200  $\mu$ m core, 0.39 NA), set to a power that induced a post-synaptic response of a few hundreds of pA (typically 5–10 mW), and controlled through triggering by a Digidata 1440A (Molecular Devices). For experiments comparing amplitude of postsynaptic responses between sham and SNI mice, the laser power was maintained at a consistent power for all experiments (~5 mW at tip of fibreoptic cannula). Pulses were delivered once per 15 s for 5 ms. Electrophysiological data was collected by an Axopatch 200B (Molecular Devices) or a Multiclamp 700b (Molecular Devices) connected to a PC computer equipped with Clampex 10.7 (Molecular Devices).

For recordings of optically evoked excitatory postsynaptic currents (oEPSCs), resting membrane potential was maintained at  $-60$  mV to isolate excitatory current. For recording of optically evoked inhibitory post-synaptic currents (oIPSCs), resting membrane potential was maintained at 0 mV to isolate inhibitory current. Junction potential was calculated to be 10.4 mV, such that  $-60$  mV =  $-70.4$  mV (Junction Potential Calculator, Clampex 10.4, Molecular Devices). For all experiments, reported values are not junction potential corrected. All analysis of oEPSCs/oIPSCs was performed in Clampfit 10.7 or 10.4 (Molecular Devices).

For pharmacology experiments, the following chemicals were perfused individually, or in several different combinations for 15 min after baseline recordings were performed: TTX (500 nM), 4-AP (100  $\mu$ M), Bicuculline (10  $\mu$ M), DNQX (20  $\mu$ M). Unless otherwise stated, all chemicals used were obtained from Millipore-Sigma.

### Immunohistochemistry

Mice were anesthetized with a lethal dose of isoflurane, and then transcardially perfused with 0.1 M PBS, followed by 4% PFA in PBS. Brains were then extracted, and post-fixed in 4% PFA in PBS for 2 h at room temperature, and then transferred to 30% sucrose in PBS at 4°C. Brains were then mounted in OCT, and frozen on dry ice for sectioning. Coronal sections (40  $\mu$ m thickness) of the vPAG and LC (bregma  $-5.7$  to  $-4.2$ ) were collected using a cryostat (Leica CM3050 S) into wells containing 30% sucrose in PBS. Slices were then washed three times with PBS and placed into blocking/permeabilizing solution for 90 min (2% bovine serum albumin, 3% normal donkey serum, 0.3% Triton, in PBS). Following this, slices were placed into primary incubation overnight at room temperature on a rocker (Rocking Platform 200, VWR). Primary incubation solution was as above, but with 1% BSA. The next day, slices were washed three times with PBS and then placed into secondary incubation for 3 h (same as primary incubation solution). Slices were then washed a final three times, with DAPI (1:1000) included in the second last wash and mounted on Superfrost slides (Fisher Scientific) with Fluoromount (Cedarlane). Negative controls lacking primary antibody were run with each cohort of experiments. All chemicals unless otherwise specified were obtained from Sigma Aldrich. Antibody dilutions were as follows: Primary - Sheep TH (1:500), Mouse CaMKII (1:100), Rabbit GABA (1:300); Secondary - Donkey anti-sheep 647 (1:500), Donkey anti-mouse 568 (1:1000), Donkey anti-mouse 647 (1:1000), Donkey anti-rabbit 647 (1:500).

Images were taken on a Leica TCS SP8 confocal microscope at either 2.5 $\times$  (0.07 NA), 5 $\times$  (0.15), 20 $\times$  (0.75 NA), or 63 $\times$  (oil immersion, 1.4 NA). Quantitative analysis was only performed on images obtained at 20 $\times$ . Average laser settings were as follows: 405 nm excitation (DAPI), 410–480 nm emission, 0.5–1% intensity; 488 nm excitation (CTB-488), 495–540 nm emission, 3.5–4% intensity; 570 nm excitation (for 568 secondary or for ai9 fluorescence), 575–640 nm emission, 0.5–2.5% intensity, 645 nm excitation (for 647 secondary), 650–780 nm emission, 1.5% intensity. Gain was always set to 100%, and gating was varied from 0.6 to 0.8 – 6.0–8.0. Images were always obtained at 2048  $\times$  2048 pixels, 12-bit depth, with z-steps of 1.5  $\mu$ m, and frame averaging of 6–8x.

Analysis of co-localization and cell counts was performed blinded to condition or sex wherever possible, and counts per slices were averaged over 4–6 slices per mouse with even bregma spacing. Individual data values reported within this manuscript represent averages across a single mouse representing 200–500 individual neuron counts. When determining tdTomato positivity both for GAD2-Cre and VGLUT2-Cre mouse lines, dense labeling of the vPAG neuropil was noted. Therefore, strict criteria were used to define tdTomato positivity. This included the presence of positive signal across the entire cell body, extending to CTB staining, and slightly decreased signal at one puncta within the cell body, likely representing the nucleolus.

### RNAscope *in situ* hybridization (ISH)

Fixed slices of vPAG tissue (bregma  $-5.0$  to  $-4.2$ ) were prepared as for immunohistochemistry, except with slices obtained with 20  $\mu$ m thickness. Slices were stored in 30% sucrose in PBS at 4°C until RNAscope was performed.

ISH was performed using the RNAscope Multiplex kit (#323110, ACD) following the initial steps of the protocol published by Gabrinski et al. with minor modifications.<sup>61</sup> Briefly, free floating sections were washed four times in tris-buffered saline (TBS), incubated in H<sub>2</sub>O<sub>2</sub> (ACD #322381), rinsed again, and mounted directly on Histobond slides (VWR, #16004-406). The sections were then dried overnight at 60°C. From this point, the ACD RNAscope Multiplex Fluorescent Detection Reagent V2 protocol was followed to detect the following targets using ACD probes: Gad2 (#439371-C1), Slc17a6 (319171-C2; VGAT), and Slc32a1 (ref. 319191-C3; VGLUT2). Opal dyes were used for channels as follows: Opal 620 for Channel 1, Opal 570 for Channel 2, and Opal 690 for Channel 3. Negative controls were performed using a probe against DapB (of *Bacillus subtilis* strain) (ACD #320871). Positive controls were performed using a 3-plex Positive Control Probe (#320881) against Polr2a (C1 channel; moderate to low expressor target), PPIB (C2 channel, moderate-high), and UBC (C3 channel, highest). As controls

for potential imaging channel bleed-through, dentate gyrus slices were also collected and imaged alongside vIPAG and LC slices. Slices were treated with DAPI prior to mounting on coverslips with Fluoromount for imaging on confocal.

Criteria for RNAscope quantification were as follows: Only puncta that overlapped with DAPI signal were included in quantification, and at least 2 puncta had to be present and overlapping with DAPI signal for positive identification. Dotted lines in the figures were drawn slightly outside the DAPI margins so as to not obscure the DAPI signal from reader visualization.

Images were taken on a Leica TCS SP8 white light confocal microscope at either 2.5× (0.07 NA), 5× (0.15), 20× (0.75 NA), or 63× (oil immersion, 1.4 NA). Quantitative analysis was performed on images obtained at 20×. Average laser settings were as follows: 405 nm excitation (DAPI), 410–480 nm emission, 0.5–1% intensity; 488 nm excitation (CTB-488), 495–540 nm emission, 2.5% intensity; 550 nm excitation (Opal 570), 555–580 nm emission, 1% intensity, 590 nm excitation (Opal 620), 595–640 nm emission, 0.75% intensity; 670 nm excitation (Opal 690), 675–780 nm emission, 0.75% intensity. Gain was always set to 100%, and gating was varied from 0.6 to 0.8 – 6.0–8.0. Images were always obtained at 2048 × 2048 pixels, 12-bit depth, with z-steps of 1.5 μm, and frame averaging of 6–8x.

### QUANTIFICATION AND STATISTICAL ANALYSIS

Statistical analysis of two groups were performed as unpaired t-tests where data were normally distributed, or as Mann-Whitney tests where data failed the Shapiro-Wilk test ( $\alpha > 0.05$ ). One-way ANOVAs were performed on data comprising three or more groups, with post-hoc Sidak's comparisons. All one-way ANOVAs performed met criteria for assumption of normality. Two-way ANOVAs were performed where two or more variables were measured, with post-hoc Sidak's comparisons.

All analysis and data visualization were performed with Graphpad PRISM 9.5.1 (Graphpad software, Boston, MA, USA). In all immunohistochemistry and RNAscope graphs, data points represent individual mice, for which technical replicates were performed and averaged together. Electrophysiological data are plotted as single neurons, for which up to 10 neurons were recorded from a single mouse. Number of total mice used in each experiment are indicated in the legends. Error bars represent  $\pm$  SEM.